Analytical description of shape transition in nuclear alternating parity bands*

E. V. Mardyban[1,2;1)] T. M. Shneidman[1,3;2)] E. A. Kolganova[1,2] R. V. Jolos[1,2] S.-G. Zhou(周善贵)[4,5,6,7]

[1] Bogoliubov Laboratory of Theoretical Physics, Joint Institute for Nuclear Research, Dubna 141980, Russia
[2] Dubna State University, Dubna 141980, Russia
[3] Kazan Federal University, Kazan 420008, Russia
[4] CAS Key Laboratory of Theoretical Physics, Institute of Theoretical Physics, Chinese Academy of Sciences, Beijing 100190, China
[5] School of Physical Sciences, University of Chinese Academy of Sciences, Beijing 100049, China
[6] Center of Theoretical Nuclear Physics, National Laboratory of Heavy Ion Accelerator, Lanzhou 730000, China
[7] Synergetic Innovation Center for Quantum Effects and Application, Hunan Normal University, Changsha 410081, China

Abstract: The angular momentum dependencies of parity splitting and electric dipole transitions in the alternating parity bands of heavy nuclei have been analyzed. It is shown that these dependencies can be treated in a universal manner with a single critical angular momentum parameter, which characterizes phase transition from octupole vibrations to the stable octupole deformation. Using the simple but useful model of axially-symmetric reflection-asymmetric mode, the analytical expressions for parity splitting and electric dipole transitional moment have been obtained. The findings are in good agreement with the experimental data for various isotopes of Ra, Th, U, and Pu.

Keywords: octupole deformation, phase transition, angular momentum

PACS: 21.10.Re, 21.10.Ky, 21.60.Ev **DOI:** 10.1088/1674-1137/42/12/124104

1 Introduction

The investigation of phase transitions in nuclei has attracted much attention in recent times since the nucleus provides an opportunity to study numerous examples of this phenomenon. Mainly, the phase transitions between spherical, axially deformed, and the γ-soft limits of the nuclear structure have been analyzed [1]. Recently, the evolution of reflection asymmetric deformation in actinides and rare-earth nuclei has also started to attract notable attention. This is an interesting case of the occurrence of phase transition with angular momentum. Indeed, as was shown in [2], the evolution of parity splitting in the alternating parity bands in actinides clearly demonstrates the transition between the octupole non-deformed phase to the stable octupole deformation. This phenomenon can also be considered as an example of the excited state quantum phase transition [3].

It is well-known that many nuclei in the actinides and rare-earth mass regions are soft with respect to deformations that violate the spatial reversal symmetry. Experimentally, it is revealed by the appearance of low-lying negative parity states connected by strong (collective) odd-multipolarity transitions with the members of the ground state band [4]. Since the first observation of low energy negative parity states [5, 6], an extensive set of experimental data has been accumulated (for the review see [7]). Note also the recent experimental investigations on the reflection-asymmetry in ^{218,220}Rn and ^{222,224}Ra [8], in ^{240}Pu [9, 10], in ^{143}Ba [11] and in ^{144,146}Ba [12].

In nuclei with strong quadrupole deformation, yrast negative parity states constitute the rotational band 1^-, 3^-, 5^- ... In the case of static reflection-asymmetric deformation, these states together with the members of the ground state band form the unified band with the negative and positive parity states interleaved with each other following the rotational order, with an equal moment of inertia. However, in most even-even nuclei, at low angular momenta, the negative parity states are shifted upwards relative to their positions in a unified alternating parity band of the molecular type. This shift which is denoted by the parity splitting [13] indicates that at low angular momenta, nuclei undergo vibrational dynamics in a reflection-asymmetric degree of freedom. Indeed, the

Received 10 May 2018, Revised 28 August 2018, Published online 30 October 2018

* Supported by the RFBR (Moscow) (16-02-00068A) and the Russian Government Subsidy Program of the Competitive Growth of Kazan Federal University. S.G.Z. was partly supported by the National Key R&D Program of China (2018YFA0404402), the NSF of China (11525524, 11621131001, 11647601, 11747601, 11711540016), the CAS Key Research Program of Frontier Sciences (QYZDB-SSWSYS013), the IAEA CRP "F41033", the HPC Cluster of KLTP/ITP-CAS, and the Supercomputing Center, CNIC of CAS

1) E-mail: mardyban@theor.jinr.ru

2) E-mail: shneyd@theor.jinr.ru

©2018 Chinese Physical Society and the Institute of High Energy Physics of the Chinese Academy of Sciences and the Institute of Modern Physics of the Chinese Academy of Sciences and IOP Publishing Ltd

results of calculations within the shell-corrected liquid drop models [14, 15] and mean-field models [16–21] show that although the nuclei in these mass regions are soft with respect to the octupole deformation, they do not develop a strong minimum at non-zero values of reflection-asymmetric deformation.

Therefore, we see that although reflection-asymmetric deformation is not as stable as conventional quadrupole deformation, it is very important for the description of the structure of the excitation spectra. However, with the increase of angular momentum, parity splitting decreases and an almost unperturbed alternating parity band is formed. This means that reflection-asymmetric deformation is stabilized. Therefore, with an increase of angular momentum, the transition occurs from the reflection-symmetric to reflection-asymmetric phase. In [2] it was shown that it is possible to define the critical angular momentum at which this transition occurs.

Another observable that is sensitive to the strength of the reflection-asymmetric deformation is the reduced transition probability for the electric dipole transitions between the states of the negative parity and the ground state band. Data on angular momentum dependence of the dipole moment are not as rich as that for the energy spectra (for the review, see [4]). The electric dipole transitional moment increases with angular momentum until some critical value after which it remains almost constant. Such a behavior of the dipole moment is consistent with the idea of phase transition.

It is interesting to note that in odd-mass nuclei, the stabilization of the reflection-asymmetry occurs earlier than for their even-even neighbors. As shown in [22], an interplay between the single-particle motion and collective reflection-asymmetric degree of freedom leads to a reduction of parity splitting.

Theoretical models developed to describe nuclear reflection-asymmetry dynamics are dependent on the degrees of freedom used. This degree of freedom is related either to the octupole deformation [23, 24] or to clustering [25–27]. In the framework of these models, it is possible to obtain qualitative and quantitative descriptions of the evolution of reflection-asymmetric deformation with mass and charge number, as well as the energies of the lowest negative parity excitations and their decay properties. In the framework of the interacting boson model extended to include dipole and octupole bosons, an acceptable reproduction of experimental data is obtained [28]. In the cluster approach based on the semi-microscopical dinuclear system model, a satisfactory description of parity splitting and $E\lambda$ transition probabilities in many actinides have been obtained [29]. However, the evolution of reflection-asymmetry is difficult to analyze fully microscopically since it requires calculations up to large values of angular momentum. An attempt to perform the calculations in ^{144}Ba for the lowest positive and negative parity states has been performed in the GCM framework with angular momentum, parity and particle number projected HFB wave functions [30]. The same technique has been applied to the description of the lowest states in ^{224}Ra with the relativistic mean field wave functions [31]. We note also an interesting analysis of the octupole properties of U isotopes performed using improved Routhian surface calculations [32, 33].

Despite these difficulties, the analysis of experimental data shows that the behavior of parity splitting and transitional dipole moment with angular momentum seems to be universal. In other words, based on the general ideas related to the reflection-asymmetric mode (regardless of octupole or mass-asymmetry), one can propose a simple analytical description of the angular momentum dependence of these quantities containing a small number of the parameters with a clear physical meaning. These parameters can be further fitted to the experiment or calculation in the microscopic models. It is the aim of this paper to find such an analytical description of the angular momentum dependence of the main physical characteristics of the alternating parity bands.

2 Description of the model

2.1 Hamiltonian and eigenfunctions

Following the discussion in [34], we assume that the nucleus under consideration has a static quadrupole deformation $\langle\beta_{20}\rangle$ and is soft with respect to the axially-symmetric ($K = 0$) reflection-asymmetric vibrations. These vibrations can be generated either by the octupole or by the mass asymmetry degree of freedom. In both cases, we denote the corresponding dynamical variable by β_{30}, although in the case of the mass asymmetry degree of freedom, the contribution of the higher order odd multipolarity modes is effectively included. The intrinsic Hamiltonian describing collective motion in β_{30} for a given angular momentum I can be written as:

$$H_I = -\frac{\hbar^2}{2B}\frac{\mathrm{d}^2}{\mathrm{d}\beta_{30}^2} + V_I(\langle\beta_{20}\rangle, \beta_{30}), \tag{1}$$

where B is the effective mass. The potential energy V_I is an even function of β_{30}.

In the Hamiltonian (1), the coupling of the quadrupole and octupole modes is neglected. This coupling would lead to the angular momentum dependence of the moment of inertia of the octupole mode and to the K-mixing through the linking of the octupole mode with gamma-vibrations. Because we consider only K=0 bands in well-deformed nuclei for not too large angular momenta in this study, it seems reasonable to neglect the quadrupole-octupole couplings by using the average

values of quadrupole deformations.

The numerical diagonalization of the Hamiltonian (1) with different variants of the potential V_I has shown [25, 35] that with a good accuracy, the lowest eigenstate of the positive parity can be approximated as a superposition of two Gaussians of width $\sqrt{\hbar/(B\omega(I))}$ centered at $\beta_{30}=\pm\beta_m(I)$

$$\Psi_I^{(+)}(\beta_{30}) = \left[\frac{\omega(I)}{\pi\hbar}\right]^{1/4}\left(2\left\{1+\exp\left[-\frac{B\omega(I)}{\hbar}\beta_m^2(I)\right]\right\}\right)^{-1/2} \times\left(\exp\left[-\frac{B\omega(I)}{2\hbar}(\beta_{30}-\beta_m(I))^2\right]+\exp\left[-\frac{B\omega(I)}{2\hbar}(\beta_{30}+\beta_m(I))^2\right]\right), \quad (2)$$

where, $\omega(I)$ is, in principle, a function of the angular momentum which is determined further. The convenience of the ansatz (2) for the positive parity wave functions is because both the limit of the octupole vibrations and the limit of the stable octupole deformation are described equally well by the ansatz [34]. One can introduce the parameter

$$\xi_I=\sqrt{\frac{B\omega(I)}{\hbar}}\beta_m(I), \quad (3)$$

which gives the ratio of a distance between the centers of the Gaussians to the sum of their widths. If $\xi\ll 1$, the overlap of the components in (2) is large and the wave function $\Psi_I^{(+)}$ corresponds to the case of octupole vibrations. If $\xi\gg 1$, the situation is the opposite and the components in (2) are well-separated. The latter corresponds to the static octupole deformation.

With the wave function $\Psi_I^{(+)}$, one can obtain the potential for the axially-symmetric octupole mode from the Schrödinger equation with the Hamiltonian (1) as:

$$V_I(\langle\beta_{20}\rangle,\beta_{30})=\frac{\hbar^2}{2B}\frac{\Psi_I^{(+)''}}{\Psi_I^{(+)}}+E_I^{(+)}(\langle\beta_{20}\rangle), \quad (4)$$

where $E_I^{(+)}(\langle\beta_{20}\rangle)$ is the excitation energy of the lowest state with an angular momentum I and a positive parity. In this investigation, we are interested in the calculation of the parity splitting which is determined as a difference between the energies of the negative parity $E_I^{(-)}$ and the positive parity $E_I^{(+)}$ states with the same angular momentum I. Since there exists only one physical excited state for a given I (positive parity for even I and negative parity for odd I) due to the $K=0$ selection rules, an experimental parity splitting can be determined as a difference between the experimental excitation energy for one parity and the energy obtained by interpolation between the energies of the neighboring states of the opposite parity (see [13] or Eq. (34) of the present paper). Thus, $E_I^{(+)}(\langle\beta_{20}\rangle)$ never enters the final results and we can set it equal to zero. Note, however, that as discussed in Sect. (3.2), this can only be done for the well-deformed nuclei.

The ansatz (2) for the wave function $\Psi_I^{(+)}(\beta_{30})$ yields the following expression for the potential energy of the axially-symmetric reflection-asymmetric mode determined up to I-dependent constant

$$V_I(\beta_{30}) = \frac{\hbar\omega}{2}\left(-1+\frac{B\omega(I)}{\hbar}(\beta_{30}^2+\beta_m^2) -2\frac{B\omega(I)}{\hbar}\beta_m\beta_{30}\tanh\frac{B\omega(I)}{\hbar}\beta_m\beta_{30}\right). \quad (5)$$

The potential (5) is used for the numerical diagonalization of H_I and to calculate the parity splitting as a function of angular momentum.

Using the dimensionless variable $x=\beta_{30}/\beta_m(I)$ and the parameter ξ defined in Eq. (3), one can rewrite the Hamiltonian H_I and the potential energy V_I in a convenient form as follows:

$$\begin{aligned} H_I &= \hbar\omega(I)h(\xi_I),\\ h(\xi) &= -\frac{1}{2\xi^2}\frac{d^2}{dx^2}+v_\xi(x),\\ v_\xi(x) &= \frac{1}{2}(\xi^2-1)+\frac{1}{2}\xi^2x^2-\xi^2x\tanh(\xi^2x). \end{aligned} \quad (6)$$

From Eq. (6) it follows that the parity splitting can be parametrized as

$$\Delta E(I)\equiv E_I^{(-)}-E_I^{(+)}=\hbar\omega(I)f(\xi_I), \quad (7)$$

where $f(\xi_I)$ is the energy of the first-excited state of the Hamiltonian $h(\xi)$ (the ground state energy of this Hamiltonian is zero). All nuclear specific information is contained in the dependence of ξ_I on the angular momentum and implicitly enters the Hamiltonian h_ξ and the function $f(\xi_I)$. Due to its universal character, it make sense to determine an approximate analytical expression for $f(\xi_I)$.

For small values of angular momentum ($\xi\ll 1$), the potential energy $v_\xi(x)$ reduces to that of an oscillator:

$$v_\xi(x) = \frac{1}{2}(\xi^2-1)+\frac{1}{2}(1-2\xi^2)\xi^2x^2, \quad \xi\ll 1. \quad (8)$$

The energy of the first excited state is then given by the frequency of an oscillator and we have:

$$f(\xi)=1-\xi^2. \quad (9)$$

For large values of angular momentum ($\xi\gg 1$), $v_\xi(x)$ has the form of two oscillators separated by a large bar-

rier:

$$v_\xi(x) = \frac{1}{2}(\xi^2-1)+\frac{1}{2}\xi^2(|x|-1)^2, \quad \xi\gg 1. \tag{10}$$

The value of the energy interval between the two lowest levels of the double well potential for a large barrier is given as [36]

$$f(\xi)=\frac{2}{\sqrt{\pi}}\xi\exp(-\xi^2). \tag{11}$$

Both limits, (9) and (11), are reproduced by one general expression:

$$f(\xi) = \frac{\xi^2 \mathrm{e}^{-\xi^2}}{2\left[1+(1-\mathrm{e}^{-\alpha\xi^2})\frac{\sqrt{\pi}}{4}\xi\right]}\coth\left(\frac{\xi^2}{2}\right), \quad \text{for} \quad \alpha=0.053, \tag{12}$$

where the value of the parameter α is obtained by fitting the numerical results for the $f(\xi)$. The results obtained by numerical diagonalization of the Hamiltonian and those given by (12) are presented in Fig. 1. In the limiting cases of very small and very large ξ, the difference between the approximate and exact values of f is negligible and vanishes asymptotically. The maximum deviation approaches approximately 2% at $\xi\approx 2$.

It should be noted that for the actual description of the experimental data, one can set $\alpha=0$, which yields a simpler expression for the parity splitting as:

$$\Delta E(I)=\hbar\omega(I)\xi_I^2\mathrm{e}^{-\xi_I^2}\coth(\xi_I^2/2). \tag{13}$$

Because the values of parity splitting are small and are influenced by many effects which are not included in the model (for example, band crossing) in the region of $\xi\gg 1$, we can neglect the deviations of (13) from (12) for large values of ξ and use the expression (13).

2.2 Dipole transitions

In addition to the appearance of the low-lying negative parity states, a common property of nuclei exhibiting strong reflection-asymmetric correlations is the large values of the electric dipole transition probabilities [4]. While the absolute values of the dipole moment for the transitions between negative- and positive-parity states depend on the nucleus, its angular momentum dependence can be described, as it is shown in the following section, by the universal function. This is similar to the situation with the parity splitting.

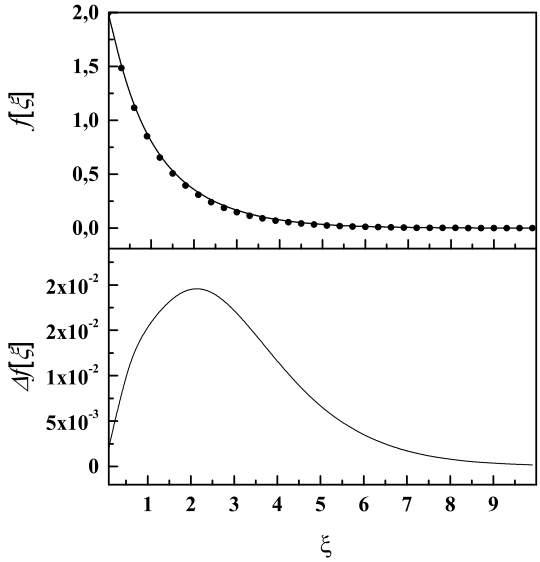

Fig. 1. Upper part: The function $f(\xi)$ obtained by the numerical diagonalization of the Hamiltonian h_I (dots) and with an approximation of Eq. (12) (solid line). Lower part: difference between exact and approximated values of function $f(\xi)$.

In the case of the well-deformed axially-symmetric nuclei, the operator of the collective electric dipole moment can be written in the intrinsic system as:

$$D_0\sim C\beta_{20}\beta_{30}, \tag{14}$$

where C is the dipole polarizability determined by the asymmetry between neutron and proton densities [4]. In the macroscopic liquid drop model, for example, we have:

$$D_0=C_{\mathrm{LD}}AZe\beta_{20}\beta_{30}, \tag{15}$$

where $C_{\mathrm{LD}}=0.0007$ fm [37].

Therefore, we see that the angular momentum dependence of the transitional dipole moment is determined by the matrix element $\langle i||\beta_{30}||f\rangle$, where vectors $|i\rangle$ and $|f\rangle$ denote the initial and final states, respectively. The lowest negative parity eigenfunction of the Hamiltonian (1) can be found numerically by solving the Schrödinger equation with potential (5). However, given that our objective is to obtain the result in the analytical form we supplemented the ansatz (2) for the positive parity ground state wave function by the expression for the lowest negative parity wave function as follows:

$$\Psi_I^{(-)}(\beta_{30}) = \left[\frac{B\omega(I)}{\pi\hbar}\right]^{1/4}\left(2\left\{1-\exp\left[-\frac{B\omega(I)}{\hbar}\beta_m^2\right]\right\}\right)^{-1/2} \times\left(\exp\left[-\frac{B\omega(I)}{2\hbar}(\beta_{30}-\beta_m)^2\right]-\exp\left[-\frac{B\omega(I)}{2\hbar}(\beta_{30}+\beta_m)^2\right]\right). \tag{16}$$

This form was confirmed based on numerical calculation. It should be noted that previously in [34], the methods based on supersymmetric quantum mechanics were used. Here, we use a simpler approach to obtain an approximate expression for parity splitting. Using the expression for the parameter ξ and a dimensionless variable x, the wave functions $\Psi^{(\pm)}(x)$ can be rewritten as:

$$\Psi^{(\pm)}(x) = \frac{\xi^{1/2}}{\beta_m^{1/2}\pi^{1/4}}\frac{1}{2^{1/2}\sqrt{1\pm\exp(-\xi^2)}} \times\left(\exp\left[-\frac{1}{2}\xi^2(x-1)^2\right]\pm\exp\left[-\frac{1}{2}\xi^2(x+1)^2\right]\right). \tag{17}$$

Using the ansatz (17) for the intrinsic wave functions of the positive and negative parity members of the alternating parity bands, we can find an analytical expression for the angular momentum dependence of the matrix element of β_{30}, namely:

$$\langle i||\beta_{30}||f\rangle = \sqrt{\frac{\hbar}{B\omega}}\frac{\sqrt{2}\mathrm{e}^{\frac{(\xi_f^2-\xi_i^2)^2}{2(\xi_f^2+\xi_i^2)}}(\xi_f\xi_i)^{1/2}}{\sqrt{(\mathrm{e}^{\xi_f^2}-1)(\mathrm{e}^{\xi_i^2}+1)}} \times\frac{\left(\xi_f^2-\xi_i^2+\mathrm{e}^{\frac{2\xi_f^2\xi_i^2}{\xi_f^2+\xi_i^2}}(\xi_f^2+\xi_i^2)\right)}{(\xi_f^2+\xi_i^2)^{3/2}}. \tag{18}$$

The last expression can be simplified if we assume the approximation $\xi_i\approx\xi_f=\xi$. Then

$$\langle i||\beta_{30}||f\rangle=\sqrt{\frac{\hbar}{B\omega}}\frac{\xi\mathrm{e}^{\xi^2}}{\sqrt{\mathrm{e}^{2\xi^2}-1}}. \tag{19}$$

From Eq. (19), it is seen that in the vibrational limit of the octupole motion ($\xi\ll1$), we have:

$$\langle i||\beta_{30}||f\rangle\approx\sqrt{\frac{\hbar}{B\omega}}. \tag{20}$$

For large values of ξ, the dipole moment is an increasing function of ξ. This increase is almost linear for $\xi>1$

$$\langle i|\beta_{30}|f\rangle \approx \beta_m, \qquad (\xi\gg1). \tag{21}$$

The angular momentum dependence of the dipole reduced transition probability has the form:

$$B(E1,i\to f)=B(E1,0^+\to1^-)\frac{\xi^2\mathrm{e}^{2\xi^2}}{\mathrm{e}^{2\xi^2}-1}, \tag{22}$$

where $\xi=\sqrt{\xi_i\xi_f}$.

3 Results of calculations

From Eq. (7), it follows that the angular momentum dependence of the parity splitting is determined by the function $f[\xi(I)]$. All information on the nucleus is contained in the actual dependence of ξ on the angular momentum, while the function $f[\xi]$ is universal. This function can be obtained numerically as the energy of the first excited state of the Hamiltonian h_ξ. $f[\xi]$ is approximately given by Eq. (12). Therefore, in the following, we use the function $f[\xi]$ given by Eq. (12) to describe the parity splitting of the nuclei.

Our calculations have shown that with sufficiently good accuracy that the angular momentum dependence of $\hbar\omega_I$ and ξ_I can be fitted as:

$$\hbar\omega_I=\text{const}, \qquad \xi(I) = cI. \tag{23}$$

This parametrization contains a very small number of parameters. If this parametrization of the potential is used, it can be seen that the value of the frequency $\hbar\omega$ is immediately determined by the value of the parity splitting at zero angular momentum, $\Delta E_{\exp}(0)$. Indeed, if $I=0$ then $\xi(0)=0$ and $V_I(\beta_{30})$ reduces to the oscillator potential. The interval between the ground state and the first excited state is then given by the frequency $\hbar\omega$. Therefore, we obtain that $\hbar\omega=\Delta E_{\exp}(0)$. The function $f[\xi(I)]$ is a universal function of ξ and thus depends only on the parameter c defined in Eq. (23). Moreover, if we use the results of [2], we can connect the value of c to the value of the critical angular momentum I_{crit}, at which the phase transition from the octupole nondeformed to the octupole deformed shape takes place, namely:

$$cI_{\text{crit}}=\frac{1}{\sqrt{2}}. \tag{24}$$

Finally, we obtain:

$$\Delta E(I)=\Delta E_{\exp}(0)f\left[\frac{I}{\sqrt{2}I_{\text{crit}}}\right]. \tag{25}$$

The choice of the angular momentum dependence of ξ, given by (23), can be qualitatively justified in the following way. At a low angular momentum ($I<I_{\text{crit}}$), we can consider the alternating parity band as being formed from two distinct bands consisting of even-parity and odd-parity states. Defining the moment of inertia of the positive- (negative-) parity bands as $\Im_e(\Im_o)$, the parity splitting can be obtained as:

$$\Delta E(I) = \Delta E(0)+\frac{\hbar^2I(I+1)}{2\Im_o(I)}-\frac{\hbar^2I(I+1)}{2\Im_e(I)} = \Delta E(0)-\frac{\hbar^2I(I+1)}{2\tilde{\Im}(I)}, \tag{26}$$

where

$$\tilde{\Im}(I)=\frac{\Im_e(I)\Im_o(I)}{\Im_o(I)-\Im_e(I)}. \tag{27}$$

At low I, we have an expression for the moment of inertia of the positive parity states that is given by $\Im_e(I)\approx\Im(\beta_{30}=0)$. The moment of inertia of the negative parity state $\Im_o(I)$ is a weakly dependent function of

the angular momentum [38]. Comparing (26) with the approximated expression obtained using (9), we get:

$$\Delta E(0)=\hbar\omega, \qquad \hbar\omega\xi^2(I)=\frac{\hbar^2 I(I+1)}{2\tilde{\Im}(I)}. \tag{28}$$

Because $\Im_o$, and therefore $\tilde{\Im}$ are weakly dependent functions of I, the expression (28) is in agreement with the approximation (23).

At the limit of large angular momenta ($I \gg I_{\rm crit}$) the nucleus approaches the static octupole deformation and the assumption of two separate rotational bands for positive- and negative-parity states is no longer valid. In this limit, the nuclear potential energy surface as a function of β_{30} has two pronounced minima separated by the barrier [see Eq. (10)]. The parity splitting can then be determined as [36]

$$\Delta E(I)=\frac{2\omega}{\sqrt{\pi}}\sqrt{\frac{2V_0}{\hbar\omega}}\exp\left(-\frac{2V_B}{\hbar\omega}\right), \tag{29}$$

where V_B is the barrier between the right and left octupole minima. This barrier arises because the nuclear moment of inertia increases with β_{30}. Because it is assumed that at $I=0$ the potential has the form of an oscillator [i.e. $V_B(I=0)=0$], the barrier height can be determined as the difference between the rotational energies associated with the change in the moment of inertia with β_{30}

$$V_B(I)=\frac{\hbar^2 I(I+1)}{2\Im(\beta_{30}=\beta_m)}-\frac{\hbar^2 I(I+1)}{2\Im(\beta_{30}=0)}. \tag{30}$$

For a large angular momentum, the moment of inertia of negative and positive parity states are both close to the value at the minimum of the potential, i.e. $\Im(\beta_{30}=\beta_m)\approx\Im_o$. Therefore, we have

$$V_B(I)=\frac{\hbar^2 I(I+1)}{2\tilde{\Im}(I)}. \tag{31}$$

Comparing the expression (29) with the barrier height in the form (31) with the expression (11) we obtain:

$$\Delta E(0)=\hbar\omega, \hbar\omega\xi^2(I)=\frac{\hbar^2 I(I+1)}{\tilde{\Im}(I)}, \tag{32}$$

where the constancy of $\hbar\omega$ is again taken into account.

As $\tilde{\Im}$ is a weakly dependend function of I, the assumption (23) is approximately valid in both limits of small and large angular momenta. With the help of (23), (24) and (28), the critical value of the angular momenta can be related to the change in the rotational energy caused by the mass asymmetric deformation dependence of the moment of inertia

$$I_{\rm crit}=\gamma\left(\frac{\Delta E(0)}{2\hbar^2}\frac{\Im_0\Im_e}{\Im_0-\Im_e}\right)^{1/2}, \tag{33}$$

where γ is a constant close to unity. In this expression, the moment of inertia of the positive parity states should be calculated at small angular momenta, namely $\Im_e=\Im_e(I=2)$, while the moment of inertia of the negative parity states should be considered in the vicinity of the critical angular momentum $\Im_e=\Im_e(I=I_{\rm crit})$.

Using the procedure described in [2], we can calculate the barrier separating the octupole minima as a function of angular momentum. The result is shown in Fig. 2. Similarly to the parity splitting, which was represented as a function of $I/I_{\rm crit}$, the barrier is represented by the universal function. We see that up to the critical value ($I/I_{\rm crit}=1$), there is no barrier ($V_B=0$). Beyond the critical value, the barrier starts to grow quadratically in accordance with Eq. (31).

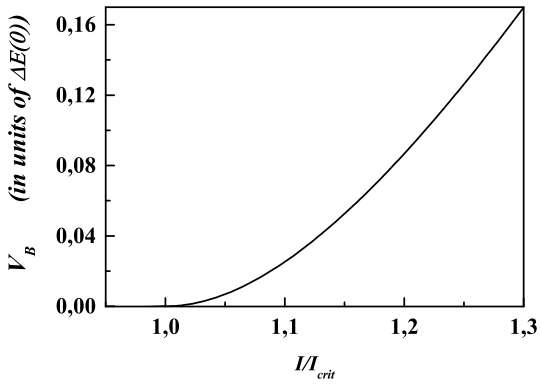

Fig. 2. The barrier separating the octupole minima as a function of angular momentum. There is no barrier ($V_B=0$) for values of angular momenta smaller than the critical ($I/I_{\rm crit}\leq 1$).

The calculation of the parity splitting is performed with the use of the expression (25) with the function f in the form (12). The experimental values for the parity splitting $\Delta E(I)$ are determined using the experimental energies $E_{\rm exp}(I)$ of the lowest negative parity states and the positive parity states of the ground state band [39]. The quantity $\Delta E(I)$ is determined as the difference between the energies of the negative- and the positive-parity states with the same spin I. As described in the preceding section, since at every value of I there exists only one state with the fixed parity $\pi=(-1)^I$, the energy of the state of the opposite parity but with the same I can be determined only by interpolation using the energies of the neighboring states of I. This interpolation should account for the angular momentum dependence of the excitation energy near I. Since it is assumed that nuclei have a stable quadrupole deformation in the model, the rotational law can be used, which leads to the following interpolation [40]:

$$E_{\rm inter}(I+1)=\frac{1}{2}[E_{\rm exp}(I+2)+E_{\rm exp}(I)] -\frac{1}{8}[E_{\rm exp}(I+4)-2E_{\rm exp}(I+2)+E_{\rm exp}(I)], \tag{34}$$

and the parity splitting is given by

Table 1. The values of the parameters $\Delta E(0)$ (keV) and c used to describe the parity splitting in the alternating parity bands of various actinide are presented. Additionally, the last column contains the values of the critical angular momenta $I_{\rm crit}$ characterizing the phase transition from octupole vibrations to the stable octupole deformation.

nucleus	$\Delta E(0)$/MeV	c	$I_{\rm crit}$	nucleus	$\Delta E(0)$/MeV	c	$I_{\rm crit}$
^{222}Ra	0.209	0.252	2.81	^{238}Pu	0.584	0.053	13.32
^{224}Ra	0.192	0.210	3.37	^{240}Pu	0.585	0.058	12.10
^{226}Ra	0.235	0.150	4.70	^{242}Pu	0.767	0.060	11.77
^{228}Ra	0.456	0.094	7.53	^{244}Pu	0.888	0.047	14.94
^{224}Th	0.226	0.247	2.86	^{230}U	0.351	0.063	11.21
^{226}Th	0.209	0.149	4.88	^{232}U	0.548	0.044	16.20
^{228}Th	0.311	0.094	7.54	^{234}U	0.772	0.031	22.90
^{230}Th	0.492	0.069	10.21	^{236}U	0.674	0.046	15.39
^{232}Th	0.699	0.049	14.50	^{238}U	0.669	0.056	12.67
^{234}Th	0.685	0.060	11.77	^{240}U	0.789	0.058	12.12

$$\Delta E(I)_{\rm exp}=(-1)^I(E_{\rm inter}(I)-E_{\rm exp}(I)). \quad (35)$$

An alternative expression for the parity splitting is given in [41]. Both definitions produce almost identical numerical results for the parity splitting.

Because the experimental value for the parity splitting at $I=0$ is not available, the value $\Delta E(0)$ is fixed to reproduce experimental data for $\Delta E_{\rm exp}(1)$. The critical angular momentum $I_{\rm crit}$ is fitted to give a best overall description of the parity splitting in the range of the angular momenta $0\leq I\leq 20$. Larger values of the angular momenta are not considered because of the possible appearance of the band crossing at higher values of I. The calculations performed for the deformed isotopes of Ra, Th, U, and Pu are presented in Figs. 3-6 together with the experimental data from [39]. The obtained values of the critical momenta $I_{\rm crit}$ are presented in the Table 1.

A good overall agreement with the experimental results is observed for all the considered nuclei. There are discrepancies in the behavior of the calculated and experimental dependencies for parity splitting which can be differentiated into two "groups". The discrepancies of the first group are due to the fact that the experimental parity splitting can assume negative values, while the calculated result approaches zero and remains positive. Among the considered nuclei, this is the case for ^{222,224,226}Ra and ^{224,226}Th. Such a behavior of the parity splitting results from the coupling of the axially-symmetric octupole mode to the other modes which are not included in the model. For example, all nuclei in the considered mass region have a negative parity band with $K=1$ [9]. This band can be interpreted as being built on the excitation of the non-axially symmetric octupole mode [38]. The Coriolis coupling of this band with the negative parity states of the alternating parity band shifts the latter down in energy. Since there isn't a $\Delta K=1$ partner band for the states of the positive parity, this perturbation will decrease the parity splitting and, if the unperturbed parity splitting is close to zero, it will be shifted to negative values.

The effect of Coriolis coupling with non-axially symmetric modes can only be seen in nuclei with critical angular momenta that is not too large. Indeed, the parity splitting adopts negative values only for ^{222,224,226}Ra, with critical angular momenta $I_{\rm crit}$ of 2.81, 3.37, and 4.70, respectively and for ^{224,226}Th ($I_{\rm crit}$=2.86, 4.88) .

If the critical angular momentum is large, this effect is hidden by the discrepancies of the second group. The second group combines the nuclei with large critical angular momenta, such as heavy Th isotopes and most of the considered U, and Pu isotopes (see Figs. 4–6). For these nuclei, we see that the calculated parity splitting for $I>I_{\rm crit}$ demonstrates a steeper incline than the experimental result. These discrepancies can be related to centrifugal stretching. Indeed, from Eq. (32) it follows that the linear dependence of $\xi(I)$ given by (23) can only be assumed if the reduced moment of inertia does not depend on the angular momentum. This is an obviously rather crude approximation for large values of I. To improve the agreement with the experimental results at large values of I, we can assume

$$\xi(I)=cI/(1+{\rm d}I), \quad (36)$$

instead of (23). As an example, the effect of this additional term is demonstrated by the dashed line in Fig. 5 for ^{230,232,236,238}U, whose alternating parity bands are long enough to account for the additional term in the angular momentum dependence of ξ. Thus, by adding the parameter d, the agreement between the calculated and experimental parity splitting at large angular momenta is improved. However, to keep the model simple, we avoid the introduction of an additional parameter d.

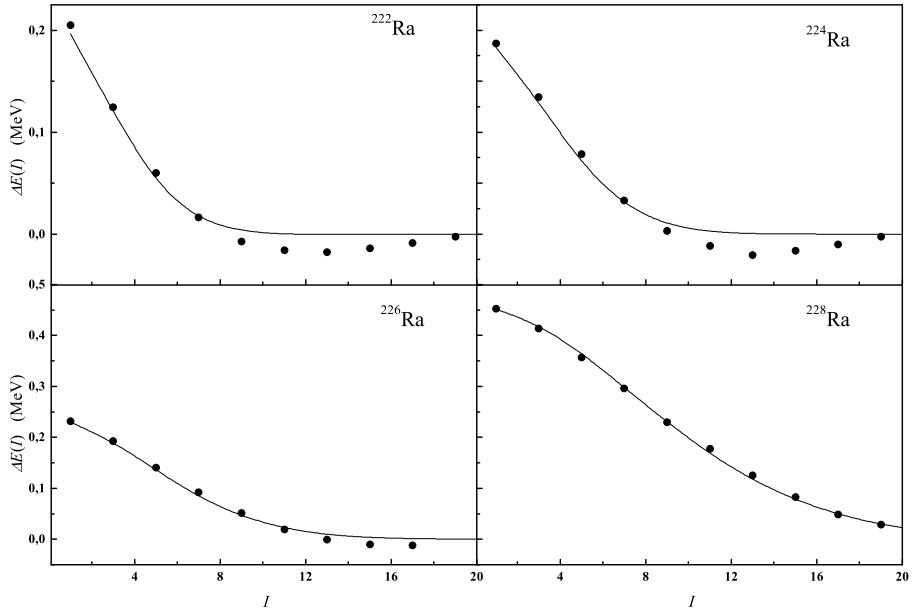

Fig. 3. Parity splitting as a function of angular momentum for various Ra isotopes. Experimental data (circles) are taken from [39]. The calculated parity splitting (lines) are obtained as in Eq. (25) with the use of the approximation (12). The values of the parameters $I_{\rm crit}$ and $\Delta E(0)$ are given in Table 1.

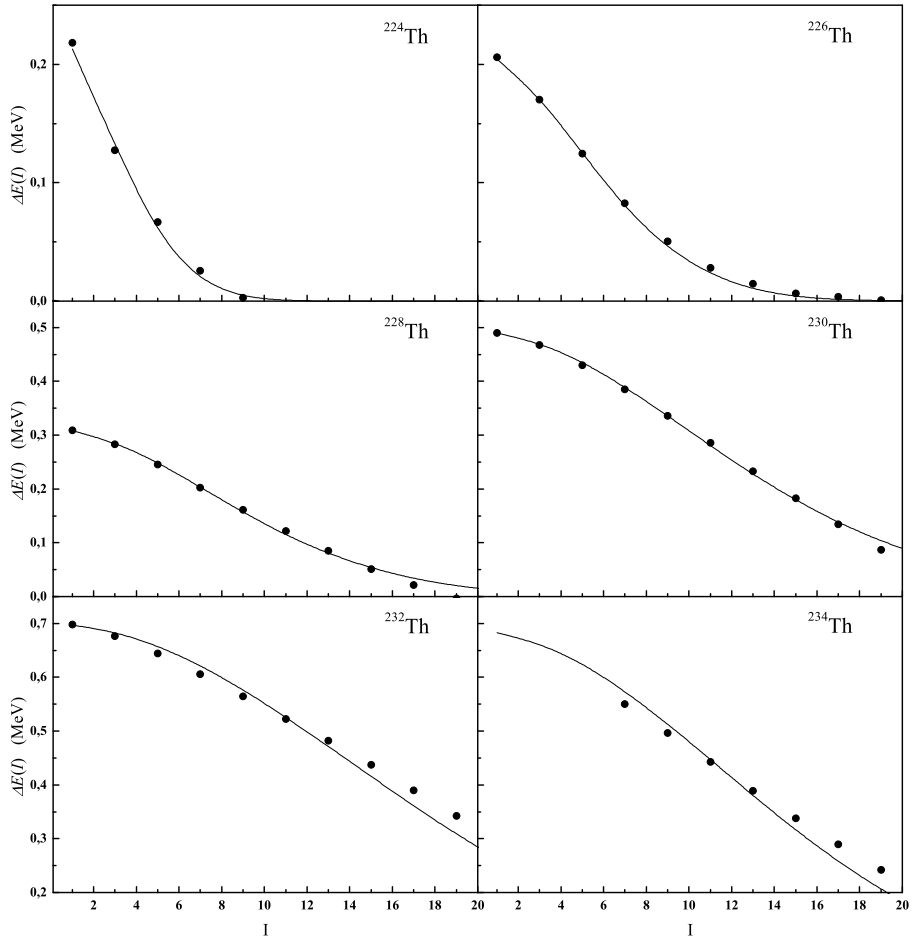

Fig. 4. Parity splitting as a function of angular momentum for various Th isotopes. Experimental data (circles) are taken from [39]. The calculated parity splitting (lines) are obtained as in Eq. (25) with the use of the approximation (12). The values of the parameters $I_{\rm crit}$ and $\Delta E(0)$ are given in Table 1.

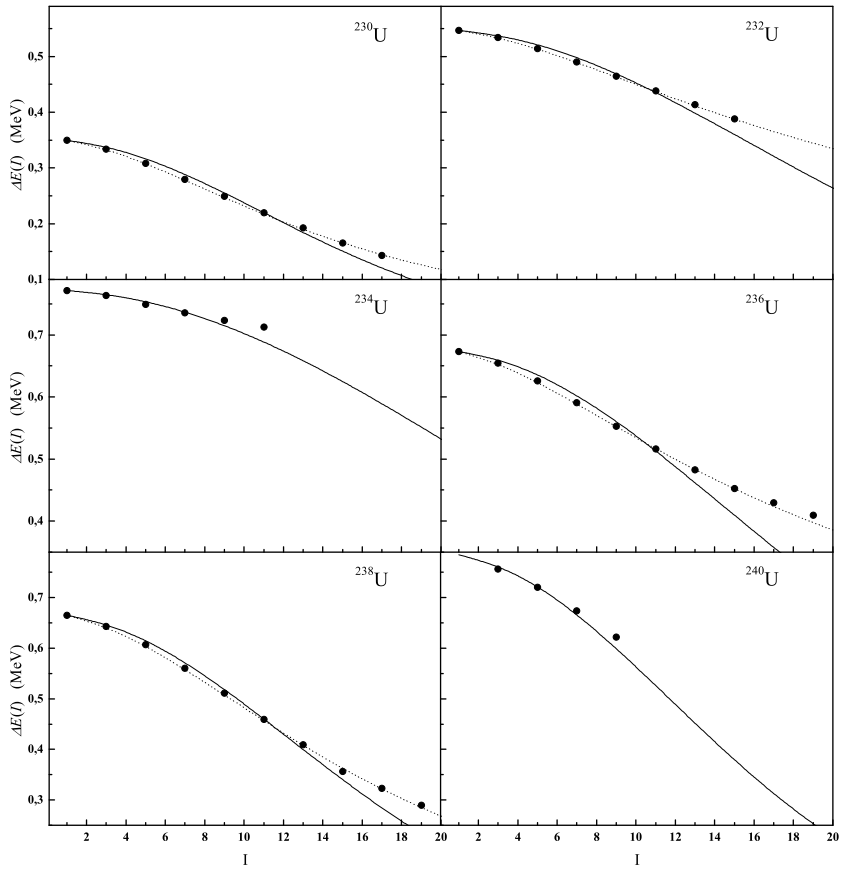

Fig. 5. Parity splitting as a function of angular momentum for various U isotopes. Experimental data (circles) are taken from [39]. The calculated parity splitting (lines) are obtained as in Eq. (25) with use of the approximation (12). The values of the parameters $I_{\rm crit}$ and $\Delta E(0)$ are given in Table 1. The calculations are performed based on the dependence of ξ on the angular momentum in the form (36) displayed by the dashed line (see discussion in the text).

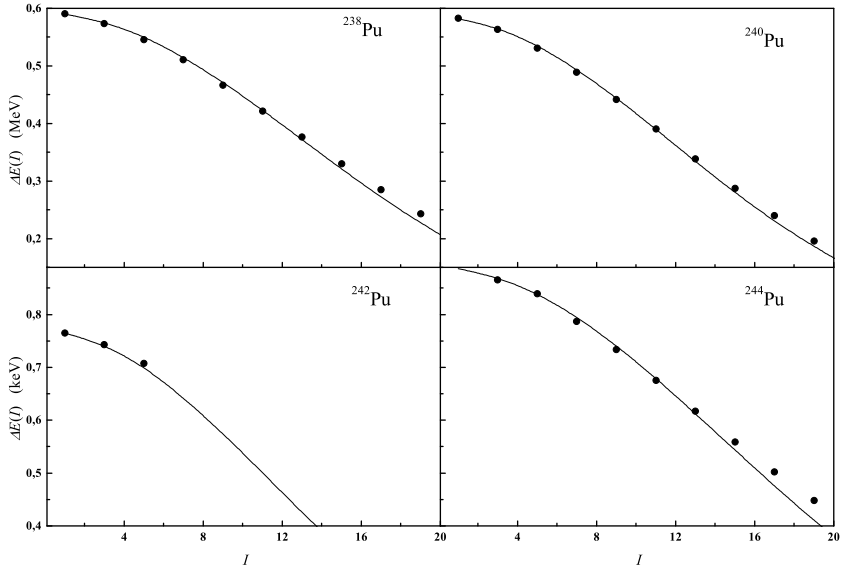

Fig. 6. Parity splitting as a function of angular momentum for various Pu isotopes. Experimental data (circles) are taken from [39]. The calculated parity splitting (lines) are obtained as in Eq. (25) with th use of the approximation (12). The values of the parameters $I_{\rm crit}$ and $\Delta E(0)$ are given in Table 1.

It is worth mentioning that for large angular momentum, one should also consider the coupling of octupole-mode with single-particle degrees of freedom. This would lead to the mixture of octupole-mode with various two quasi-particle excitations and, as a result, to band crossing. An interesting example of such a band crossing is provided by the different behavior of the parity splitting in ^{238}U and ^{240}Pu. In the low spin part, the parity partner bands behave almost the same; however, at larger spins, their behavior differs dramatically [42]. This difference can be generated by the crossing of the alternating parity band with the relatively low-lying proton two-quasiparticle positive parity band. The proton two-quasiparticle excitation could be different in both nuclei because of the difference in the positions of the proton's Fermi level. Because of the crossing, the lowest positive parity states are additionally shifted downwards, and parity splitting decreases more slowly. However, the treatment of this coupling is outside the limit of applicability of the model. For angular momenta well above the critical value, the behavior of the parity splitting and the dipole moments determined by the coupling of various single-particle and collective modes and the separation of a single octupole mode is no longer valid.

Using the acquired values of the critical angular momenta $I_{\rm crit}$, one can calculate the angular momentum dependence of the electric dipole transitional moment. In Fig. 7, the results for the ^{240}Pu are presented. The calculated values are compared with the experimental data on dipole moment obtained in [43]. In order to obtain the values of D_0 from the experimental data, we have assumed the stable quadrupole deformation and an axial shape of the considered nuclei.

The dipole moment is obtained from the reduced transition probabilities using the expression [4]

$$B(E1,I\to I') = \frac{3}{4\pi}D_0^2\left(C^{I'0}_{I0\ 10}\right)^2 = \frac{1}{2I+1}\langle I'||M(E1)||I\rangle^2. \quad (37)$$

As it follows from (22), the absolute value of D_0 requires the experimental data on $B(E1,0^+\to 1^-)$ for its definition. If these data are not available, the initial value of the dipole-to-quadrupole moment is fitted to reproduce the lowest experimentally available value of D_0/Q. As seen from the results presented in Fig. 7, the calculation performed using Eq. (22) and the critical angular momentum obtained from the fit of the parity splitting reproduces well the angular momentum dependence of the dipole transition probabilities along the alternating parity band.

Another example is presented in Fig. 8 for the reduced matrix elements of the E1 transitions in ^{226}Ra. The experimental data are taken from [44]. Unlike ^{240}Pu which remains reflection symmetric until a large angular momenta ($I_{\rm crit} = 12.1$), the ^{226}Ra has almost stable reflection-asymmetric deformation very close to the ground state ($I_{\rm crit} = 4.7$). As we see in both cases of small and large values of $I_{\rm crit}$, the calculations based on Eq. (22) agree well with the experimental data.

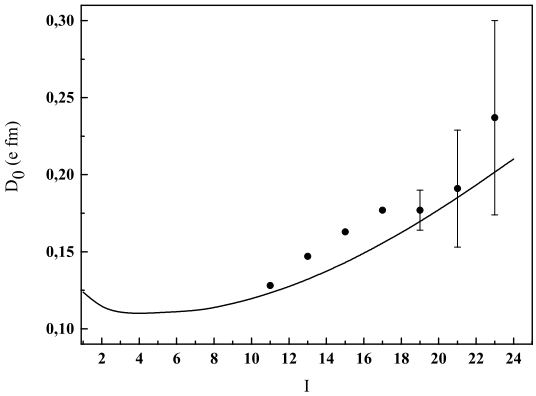

Fig. 7. Dependence of the calculated and experimental values of the transitional dipole moment on the angular momentum obtained for ^{240}Pu. The calculations are performed using the expressions (22) and (37). The value of the critical angular momentum is given in Table 1.

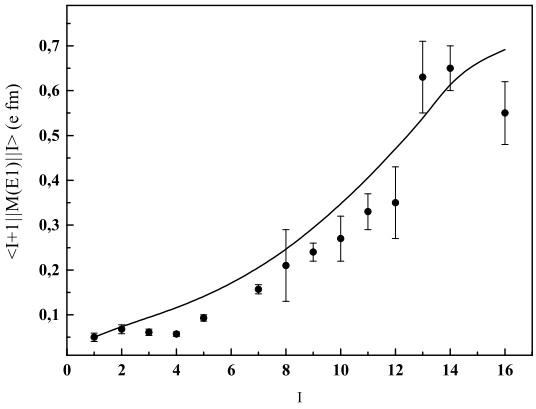

Fig. 8. Dependence of the calculated and experimental values of the $E1$ matrix element on the angular momentum for ^{226}Ra. The calculations are performed using the expressions (22) and (37). The value of the critical angular momentum is given in Table 1.

4 Conclusion

A simple model is proposed for the description of spectroscopic information on the alternating parity bands in actinides. The model is based on the assumption that the yrast negative parity states of quadrupole-deformed nuclei are related to the excitation of an axially-symmetric octupole mode. It is shown that the octupole deformation is stabilized with an increase of the angular momentum, i.e., the phase transition occurs

from octupole vibrations to the stable octupole deformation. This is caused by the dependence of the moment of inertia on the octupole deformation. As the moment of inertia increases with octupole deformation, its value is larger at the minimum of the potential than at the barrier height. As a result, the depth of the deformation minimum increases with an increase of the angular momentum. For $^{222-228}$Ra, $^{224-234}$Th, $^{230-240}$U, and $^{238-244}$Pu, the critical angular momenta $I_{\rm crit}$ characterizing the phase transition to the reflection-asymmetric shape were calculated. The relation of $I_{\rm crit}$ to the spectroscopic properties (such as the energies of the lowest $I^{\pi}=1^{-}$ states and the moments of inertia of the positive parity and negative parity bands) is obtained.

Based on this model, the approximate analytical expressions for the angular momentum dependence of the parity splitting (13) and the electric dipole transitional moment (22) were obtained. These analytical expressions contain a small number of parameters with the clear physical meaning, namely, the frequency of the axially-symmetric octupole vibrations at zero angular momentum $\hbar\omega$ and the critical angular momentum $I_{\rm crit}$. These parameters can be fitted according to the experimental data or calculated using a microscopical model. We note that the same values of the parameters $\hbar\omega$ and $I_{\rm crit}$, which were determined to provide a good agreement with the experimental data for parity splitting, provide a good description of the data for the electric dipole transitional moment. The results obtained were validated by the calculations for the different actinides and compared with the experimental data.

References

1 P. Cejnar, J. Jolie, and R. F. Casten, Rev. Mod. Phys., **82**: 2155 (2010)
2 R. V. Jolos, P. von Brentano, and J. Jolie, Phys. Rev. C, **86**: 024319 (2012)
3 F. Iachello, at 8^{th} Workshop on QPT in nuclei and other many-body systems, Praha, Czech Republic, June 6, 2016
4 P. Butler and W. Nazarewicz, Rev. Mod. Phys., **68**: 349 (1996)
5 F. Asaro, F. S. Stephens, Jr., and I. Perlman, Phys. Rev., **92**: 1495 (1953)
6 F. S. Stephens, Jr., F. Asaro, and I. Perlman, Phys. Rev., **100**: 1543 (1955)
7 I. Ahmad and P. A. Butler, Annu. Rev. Nucl. Part. Sci., **43**: 71 (1993)
8 L. P. Gaffney et al, Nature (London), **497**: 199 (2013)
9 M. Spieker et al, Phys. Rev. C, **88**: 041303(R) (2013)
10 M. Spieker et al, Phys. Rev. C, **97**: 064319 (2018)
11 X. C. Chen et al, Phys. Rev. C, **94**: 021301(R) (2016)
12 B. Bucher et al, Phys. Rev. Lett., **116**: 112503 (2016)
13 R. V. Jolos and P. von Brentano, Phys. Rev. C, **49**: R2301(R) (1994)
14 W. Nazarewicz et al, Nucl. Phys. A, **429**: 269 (1984)
15 P. Möller et al, At. Data Nucl. Data Tables, **94**: 758 (2008)
16 J. Egido and L. Robledo, Nucl. Phys. A, **494**: 85 (1989)
17 K. Rutz, J. A. Maruhn, P.-G. Reinhard, and W. Greiner, Nucl. Phys. A, **590**: 680 (1995)
18 L. M. Robledo and G. F. Bertsch, Phys. Rev. C, **84**: 054302 (2011)
19 B. N. Lu, J. Zhao, E. G. Zhao, and S. G. Zhou, Phys. Rev. C, **89**: 014323 (2014)
20 S. G. Zhou, Phys. Scr., **91**: 063008 (2016)
21 J. Zhao, B. N. Lu, E. G. Zhao, and S. G. Zhou, Phys. Rev. C, **86**: 057304 (2012)
22 G. A. Leander and Y. S. Chen, Phys. Rev. C, **37**: 2744 (2003)
23 R. G. Nazmitdinov, I. N. Mikhailov, and Ch. Briancon, Phys. Lett. B, **188**: 171 (1987)
24 N. Minkov, S. Drenska, K. Drumev, M. Strecker, H. Lenske, and W. Scheid, Phys. Rev. C, **88**: 064310 (2013)
25 T. M. Shneidman, G. G. Adamian, N. V. Antonenko, R. V. Jolos, and W. Scheid, Phys. Rev. C, **67**: 014313 (2003)
26 B. Buck, A. C.Merchant, and S. M. Perez, Phys. Rev. C, **59**: 750 (1999)
27 F. Iachello and A. D. Jackson, Phys. Lett. B, **108**: 151 (1982)
28 D. Kusnezov and F. Iachello, Phys. Lett. B, **209**: 420 (1988)
29 T. M. Shneidman, G. G. Adamian, N. V. Antonenko, R. V. Jolos, and S.-G. Zhou, J. Phys.: Conf. Ser., **569**: 012056 (2014)
30 R. N. Bernard, L. M. Robledo, and T. R. Rodriguez, Phys. Rev. C, **93**: 061392(R) (2016)
31 J. M. Yao, E. F. Zhou, and Z. P. Li, Phys. Rev. C, **92**: 041304 (2015)
32 H. L. Wang, H. L. Liu, and F. R. Xu, Phys. Scr., **86**: 035201 (2012)
33 H. L. Wang, H. L. Liu, and C. F. Jiao, Chin. Sci. Bull, **57**: 1761 (2012)
34 R. V. Jolos and P. von Brentano, Phys. Rev. C, **84**: 024312 (2011)
35 R. V. Jolos, N. Minkov, and W. Scheid, Phys. Rev. C, **72**: 064312 (2005)
36 Eugen Merzbacher, *Quantum Mechanics*, 1970
37 V. M. Strutinsky, J. Nucl. Energy, **4**: 523 (1957)
38 T. M. Shneidman, G. G. Adamian, N. V. Antonenko, R. V. Jolos, and S. -G. Zhou, Phys. Rev. C, **92**: 034302 (2015)
39 http://www.nndc.bnl.gov/ensdf
40 R. V. Jolos and P. von Brentano, Nucl. Phys. A, **587**: 377 (1995)
41 R. V. Jolos and P. von Brentano, Phys. Rev. C, **92**: 044318 (2015)
42 S. Zhu et al, Phys. Rev. C, **81**: 041306(R) (2018)
43 I. Wiedenhöver, R. V. F. Janssens, G. Hackman et al, Phys. Rev. Lett., **83**: 2143 (1999)
44 H. J. Wollersheim, et al, Nucl. Phys. A, **556**: 261 (1993)